CrystEngComm

Accepted Manuscript

ROYAL SOCIETY OF CHEMISTRY

www.rsc.org/crystengcomm

Journal Name

RSCPublishing

ARTICLE

A facile one-step fabrication of novel $WO_3/Fe_2(WO_4)_3!10.7H_2O$ porous microplates with remarkable photocatalytic activities

Cite this: DOI: 10.1039/x0xx00000x

Received 00th January 2014,
Accepted 00th January 2014

DOI: 10.1039/x0xx00000x

www.rsc.org/

Imran Aslam,[a] Chuanbao Cao,[*a] M. Tanveer,[a] M. Hassan Farooq,[b] Muhammad Tahir,[a]Syed Khalid,[a]Waheed S. Khan,[a]Faryal Idrees,[a]Muhammad Rizwan[a]and Faheem K. Butt[a]

Highly efficient visible-light-driven$WO_3/Fe_2(WO_4)_3!10.7H_2O$ porous microplates have been first time fabricated by simple one-step hydrothermal method using sodium tungstate and iron chloride as precursors. The photocatalyst was characterized by employing X-ray diffraction (XRD), field emission scanning electron microscopy (FESEM), transmission electron microscopy (TEM), X-ray photoelectron spectroscopy (XPS), UV-VIS absorption, photoluminescence (PL), and Fourier transform infrared (FTIR). From the FESEM and TEM analysis, the size of as-prepared porous microplates was estimated *ca*. 2 μm.The as-prepared sample maintained a high specific surface area (96.906 m^2/g) and showed remarkably high photocatalytic performance (k=0.06771 min^{-1})for the degradation of methyl orange (MO)under visible light irradiation. The improved performance of the product was found to be 3.3 times greater than pure WO_3 and about 6.7 times greater than that of P25 TiO_2.The enhanced optical absorption in the visible region, large specific surface area, suitable band position and efficient separation of photogenerated electron-hole pairs at the hetero junction interface between two materials were the key factors involved in the enhancement of photocatalytic activity.

Introduction

World is suffering from a serious problem of energy crises and environmental pollution these days. With the improving life style of human being, the need of clean environment, degradation of organic pollutants and effective detection of toxic and hazardous gases have become the most important issues in recent years. From the past three decades, semiconductor photocatalysis has been extensively studied and a lot of research work has been done on the fabrication of visible-light-driven semiconductor photocatalysts in order to overcome the aforesaid problems but yet it is considered one of the promising techniques to address the environmental issues like energy storage and decontamination of environmental pollution [1]. By this technique, solar energy can be utilized to decompose the organic/inorganic pollutants present in the aqueous media or air and also it can produce clean and recycle hydrogen energy as well [2, 3].Therefore, considerable attention has been paid by the researchers to develop highly efficient visible-light-driven photocatalysts due to their high utilization of solar energy, easy production and low consumption of energy [4, 5].

As an n-type semiconductor, WO_3 is of great interest for its potential applications such as electrochromic devices, field-emission devices, solar energy devices and gas sensors [6-9]. However, photocatalysis is another important application of $WO_3$where it can be utilized as a photocatalyst for the decomposition of organic pollutantsand environmental protection as well. But from the photocatalysis point of view, it has been noticed that pure WO_3 contains lower light energy conversion efficiency than that of TiO_2. The reason is that the electrons in WO_3 have low reduction potential due to its low conduction band level. The fast recombination rate of photogenerated charge carriers and low conduction band level affects the photocatalytic efficiency of pure WO_3[10] which is a big obstacle in the practical photocatalytic applications of WO_3[11]. Therefore, many attempts have been adopted to enhance the photocatalytic performance of WO_3 such as controlled morphology, doping of transition metals and composite materials etc[12]. It has been investigated that the photocatalytic activity of WO_3 can be improved by increasing the surface area and suppressing the recombination of electron-hole pairs [10]. In order to attain the increased surface area and supressed recombination of photoexcited charge carriers, most of the people has focused on the doping of metal elements into WO_3 or making its composites with other materials, such as Pd/WO_3 [13],Ag/WO_3[14],Pt/WO_3[15], $WO_3/SrNb_2O_6$ [16], V_2O_5/WO_3 [17], $CaFe_2O_4/WO_3$ [18],WO_3/g-C_3N_4[19] and $WO_3/CdWO_4$[20]etc. These newly-designed photocatalysts exhibited improved photocatalytic activity than that of the traditional ones. For example, Zhao *et* al. [10] synthesized platinum loaded WO_3 nanotubular structure as a heterocatalyst and found a promising efficiency for visible-light-driven photocatalysis. Hong *et al.*[21] fabricated heterojunction $BiVO_4/WO_3$ electrodes by

layer-by-layer deposition of WO_3 and $BiVO_4$on a conducting glass that exhibited enhanced photoactivity of water oxidation. In addition, very recently Bai *et al.*[22] synthesized the surface decorated WO_3 architectures with Fe_2O_3 nanoparticles and found remarkably high photocatalytic activity for the degradation of RhB. However, for practical or industrial applications, a photocatalyst should be of low cost and have a strong visible-light response. These modified materials still have some problems like high cost, low photocatalytic efficiency, poor stability, and so on. Therefore, it is still a great challenge to form novel, economic, well-stable and environment friendly photocatalysts with improved photocatalytic performance.

It is well known that the morphological structure of semiconductors plays crucial role in photocatalytic properties as the photogenerated electrons and holes taking part in the photocatalytic reaction are found on the surface of catalyst[23].Especially, the porous structure materials with different morphologies are of great interest and they have unique technological applications in the field of catalysis, sensing, Li-ion batteries and solar cells etc., because of their large surface area which originates from high porosity[24].In this article, we have first time demonstrated a facile route for the one-step synthesis of novel $WO_3/Fe_2(WO_4)_3$!10.7H_2O porous microplates via hydrothermal treatment. The photocatalytic activity of the as-fabricated product was investigated for the degradation of MO and the visible-light photocatalytic tests reveal that compared to pure WO_3[25],the present heterojunction/hybrid system showed excellent photocatalytic performance for the decomposition of MO molecule due to enhanced absorption in visible-light range, significant charge separation, and high transfer efficiency of photogenerated charge carriers at the heterointerface between two materials. To the best of our knowledge, this is the first report on the synthesis of a such one-step hybrid$WO_3/Fe_2(WO_4)_3$!10.7H_2O photocatalyst.The resulting hybrid system exhibited efficient photostability after four consecutive cycles. The possible mechanism regardingphotocatalyticprocess on the basis of experimental results is also discussed.

Experimental Section

Materials

All the chemicals $Na_2WO_4.2H_2O$, $FeCl_2.4H_2O$, and MO used during the synthesis process were analytical grade reagents and were used without further purification. Deionized water (DIW)was used throughout this work.

Synthesis of $WO_3/Fe_2(WO_4)_3$!10.7H_2O porous microplates

In the hydrothermal synthesis, sodium tungstate dihydrate ($Na_2WO_4.2H_2O$) and iron chloride tetrahydrate ($FeCl_2.4H_2O$) were used as precursors while deionized water as solvent. Typically, 3 mmol of ($Na_2WO_4.2H_2O$) and 1 mmol $FeCl_2.4H_2O$ were initially dissolved in 20 ml of deionized water and magnetically stirred the solution for half an hour. During the stirring, 3 mL of 3 M HCl were added dropwise to the above solution and finally a thick off white solution was transferred to a stainless- steel autoclave of 40 mL capacity. The reaction vessel was sealed and heated at 200 ˚C for 24 hours. The autoclave was then allowed to cool at room temperature and the obtained product was several times washed and centrifuged with distilled water and ethanol and then dried at 80 ˚C for 12 hours. As a result, a yellow colour powder was obtained which was preserved for further examinations. Moreover, for comparison, pure WO_3 was synthesized (see Fig. S1 (ESI†)).

Characterization

The phase characterization of as-synthesized samples were carried out by X-ray diffraction (XRD; Philips X'Pert Pro MPD), using a Cu Kα radiation source (λ= 0.15418 nm) with 2θ in the range 10° to 80°. The morphological structure, shape and size of the as-prepared samples were analysed by field emission scanning electron microscopy (FESEM), energy dispersive X-ray (EDX) analysis (Hitachi S-3500), high resolution transmission electron microscopy (TEM) JEOL JEM-2100 and X-ray photoelectron spectroscopy (XPS)Rigaku-7000 spectrometer.The well-known Brunauer–Emmett–Teller (BET) specific surface area of the as-prepared sample was measured by a Micromeritics HYA2010-C2 (Beijing Zhong Ke Hui Yu Technology Co., Ltd.) nitrogen adsorption instrument. Thermogravimetric analysis was carried out by TGA-50 Shimadzu from room temperature to 1000 °C at a constant heating rate of 10 °C min^{-1} under air atmosphere. The optical absorption spectra and energy bandgap were measured by using UV-VIS-NIR (Hitachi-4100) spectrophotometer. The room temperature PL spectrum was investigated with a fluorescence spectrometer (Hitachi FL-4500) and Fourier transform infrared (FTIR) spectra of samples were measured using a Nicolet Avatar-370 spectrometer.

Photocatalytic test

The photocatalytic activities of the as-fabricated material were carried out by decomposing the methyl orange (MO), one of the commonly used organic dyes, under visible light irradiation(λ >420 nm).In order to study the photodegradation, 100 mg of the catalyst was dispersed into an aqueous solution of MO (100 mL, 1×10^{-5} mol/L). A 500 W xenon lamp (TrusTech, CHF-XM-500W)with 420 nm cutoff filter and 300 mW/cm average visible light intensity was used for visible light irradiation source. Before exposing to light, the solution was kept under continuous magnetic stirring in dark for one hour to attain the adsorption–desorption equilibrium between the photocatalyst and organic dye. Took 5 mL of the solution after certain time intervals and centrifuged to separate the photocatalyst powder every time before measuring the absorption spectra. The variation in optical absorption spectra of the filtered solution was measured by using aUV-VIS-NIR (Hitachi U-4100) spectrophotometer. The initial concentration (C_0)was recorded the maximum absorption peak at 464 nm for MO.

Detection of hydroxyl radicals

The amount of hydroxyl radicals (˙OH) was measured according to the literature[26].Typically, 50 mg of the catalyst material were mixed in 50 mL of an aqueous solution of 3×10^{-3}M terephthalic acid (TA) and 10×10^{-3}M NaOH. This mixture was kept in the dark for 30 min under constant magnetic stirring before exposing to visible light irradiation (the same source was used for visible light irradiation as for the photocatalytic tests). Took 5 mL of the suspension after every 10 minutes and centrifuged before measuring the fluorescence test.

The photo-generated ·OH radicals react with TA to form 2-hydroxyterephthalic acid (TAOH) and show a characteristic fluorescence peak at 426 nm. The fluorescence spectrophotometer (Hitachi FL-4500) was employed to analyze the fluorescence spectra of the generated 2-hydroxyl terephthalic acid (TAOH). The excitation light of wavelength320 nm was set during the measurements of fluorescence signals. An increase in the fluorescence intensity is directly associated with the increase inamount of photo-generated ·OH radicals.

Results and discussion

Phase characterization and morphology

The phase and morphological structure of the as-prepared sample was characterized by X-ray diffraction. Fig. 1 (a)shows the typical XRD pattern of the as-synthesized $WO_3/Fe_2(WO_4)_3!10.7H_2O$; the XRD pattern can be indexed to WO_3 hexagonal phase (JCPDS Card No. 33-1387 with lattice constants $a = b = 7.298$ Å, $c = 3.899$ Å and $\alpha = \beta = 90°$, $\gamma = 120°$) with following distinctive peaks at 14.01°, 22.83°, 28.12° and 36.57° corresponding to (100), (001), (200) and (201) planes respectively. The sharp and well-defined diffraction peaks shows the high crystallinity of the material. On the other hand, there are also some peaks that are well matched with monoclinic phase of $WO_3/Fe_2(WO_4)_3!10.7H_2O$(JCPDS Card No. 23-0309) diffraction at2θ=24.26°, 2θ=28.12°, 2θ=49.8° and 2θ=58.23° corresponding to (110), (200), (220) and (400) planes respectively. The peaks of both the materials have been marked separately in the XRD pattern. An interesting fact been be noted that the main diffraction peak and some secondary peaks of WO_3 and $Fe_2(WO_4)_3!10.7H_2O$ have similar positions which suggests that both materials are well mixed/stacked with each other.

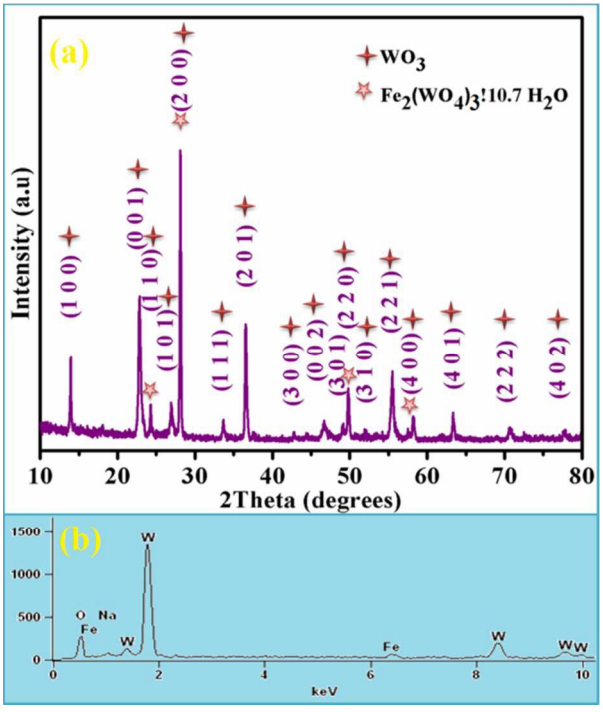

Fig. 1 (a) Typical XRD pattern and (b)EDX spectrum, of $WO_3/Fe_2(WO_4)_3!10.7H_2O$ (24 h).

Fig. 1 (b) indicates the typical energy dispersive X-ray (EDX) spectrum of the as-prepared product which provides the knowledge about the elements present in the as-synthesized material. It can be noticed from Fig. 1 (b) that the as-prepared hybrid/composite $WO_3/Fe_2(WO_4)_3!10.7H_2O$ contains the elements W, O and Fe and no other impurity element was found which shows that the fabricated product is pure.

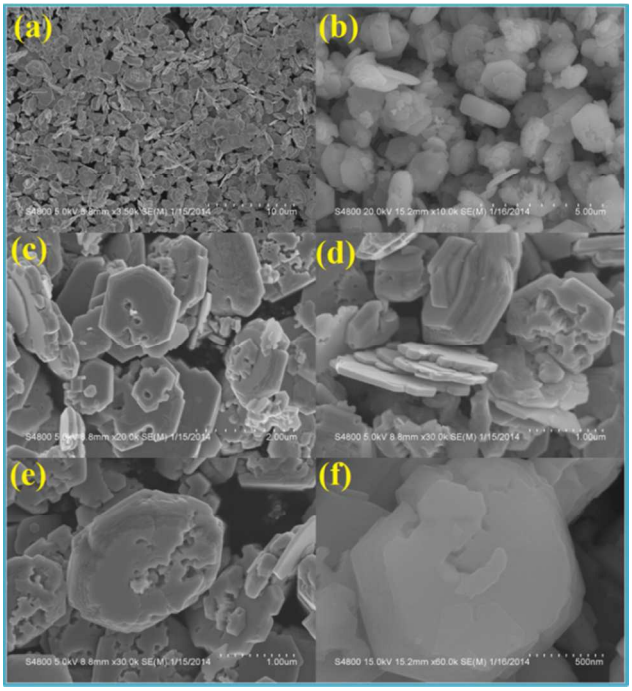

Fig. 2 (a-f)FESSEM images of $WO_3/Fe_2(WO_4)_3!10.7H_2O$ (24 h).

Fig. 2 (a-f) represents the FESEM images of the as-prepared one-step hybrid/composite $WO_3/Fe_2(WO_4)_3!10.7H_2O$ porous microplates at different magnifications. Fig. 2 shows that the as-fabricated microplates have been uniformly distributed over the surface at different orientations. The size of the microplates is in the range of about 2 µm as can be seen from Fig. 2 (c & e) while the thickness lies in the range of 100-120 nm.

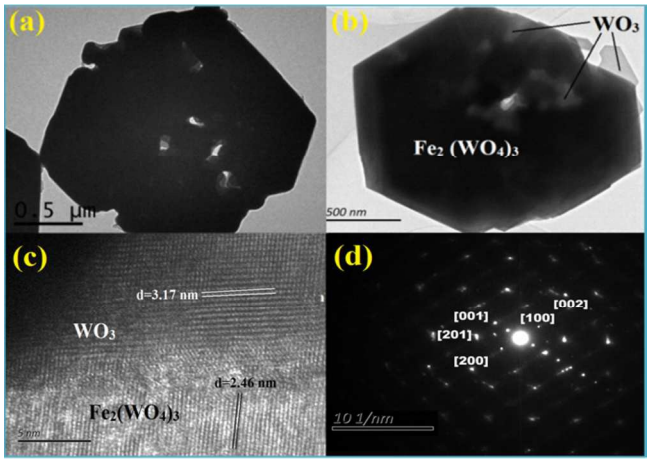

Fig. 3 (a, b)TEM images, and (c) HRTEM image, and (d) SAED pattern of $WO_3/Fe_2(WO_4)_3!10.7H_2O$ (24 h) respectively.

The size, shape and porous nature of the as-synthesized microplates can be more clearly analysed from TEM images. Fig. 3 (c) depicts the high resolution transmission electron microscopy (HRTEM) image of the final product which provides the confirmation of two different materials with specific lattice fringes in different directions. The interplanar distance of 0.317 nm corresponds to (200) crystal planes of WO_3 whereas 0.246 nm corresponds to (200) of iron oxide's crystal planes. Fig. 3 (d) presents the SAED pattern points are indexed corresponding to distinctive crystal planes, which reveals that the as-prepared product is a composed of two materials as it contains two different types of pattern.

In order to understand possible growth mechanism of the porous microplates, the time dependent experiments were performed. The time was varied from 6–18 hours; corresponding SEM images and XRD patterns of the synthesized products are shown in Fig. 4. The samples obtained after 6, 12 and 18 hours are labeled as S1, S2 and S3 respectively. At time 6 h,the SEM image (Fig. 4a) shows agglomerates type product. The particles at this stage are just seemed to align in some direction to obtain some shape. As the time was increased to 12 h, one can note that the formation of plates like structure started to grow (Fig. 4 b). With the further increase in time, *i.e.,* 18h, the formation of plates like became clearer and we can see that the whole product converted into plates spread over the surface (Fig. 4 c). It means that the time played important role in the formation of these microplates so we increased time further and obtained the well-ordered and uniformly distributed porous microplates as the final product at a time of 24h (Fig. 2 a-f) and is labeled as S4. Fig. 4 (d) represents the XRD patterns of the samples (at 6, 12 and 18 h)and it can be noticed that the XRD patterns shown in Fig. 4 (d) resemble to that of the final product (Fig. 1)and all the peaks are almost at the same positions. The content of $Fe_2(WO_4)_3!10.7H_2O$ in the final product can be seen in Fig. S2 (ESI†).

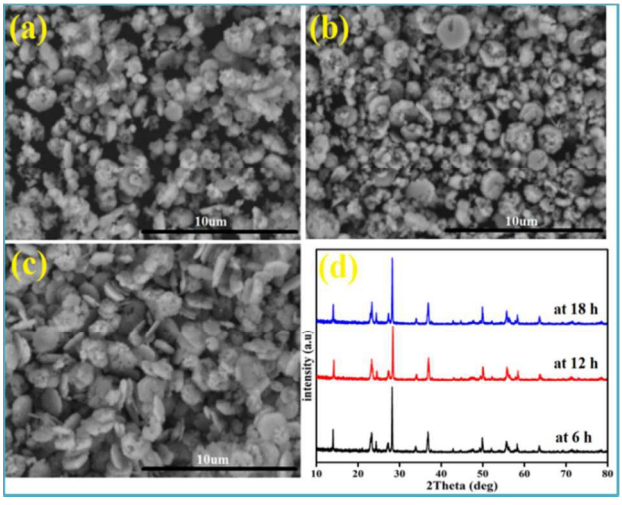

Fig. 4 SEM images of the as-synthesized product at (a) 6h, (b) 12h, (c) 18h and (d) The XRD patterns of all the samples.

XPS analysis

X-ray photoelectron spectroscopy (XPS) was employed to further confirm the surface composition and chemical states of the as-synthesized $WO_3/Fe_2(WO_4)_3!10.7H_2O$.Fig. 5 indicates the XPS spectra of the as-prepared sample which provides the knowledge about the elemental composition and surface chemical states of the final product.Fig. 5 (a) presents a low-resolution full range XPS spectrum of the as-synthesized sample is shown in Fig. 5(a). The XPS survey spectrum indicates that the distinctive as well as the Auger peaks of W,O and Fe in the fabricated material ($WO_3/Fe_2(WO_4)_3!10.7H_2O$) confirms the presence of tungsten, oxygen and iron elements only and no other peak of any impurity or byproduct was found which is in good agreement with EDX spectrum and XRD analysis. The carbon peak (C1s) appearing at 284.3 eV in Fig. 5 (b) is due to the carbon paste used during the sample preparation on the mount. The oxygen peak (O1s) centered at 529.3 eV (Fig. 5 c) could be assign to O^{-2} states oxide networks in WO_3.Fig. 5 (d) depicts the spin–orbit splitting of W4f and can be deconvoluted into a doublet with binding energy peaks at 34.8 eV and 36.9 eV resulted from the emission of $W4f_{7/2}$ and $W4f_{5/2}$ core-levels that might belong to the W^{5+}oxidation state of tungsten atoms and are in good agreement with the previously reported results[27]. Fig. 5 (e) shows the Fe 2p core-level binding energies spectrum of the as-synthesized one-step hybrid $WO_3/Fe_2(WO_4)_3!10.7H_2O$. The XPS peak positioned around about 710.8 eV can be associated with the Fe $2p_{3/2}$ level, while the binding energy peak appearing around 725.1 eV can be ascribed to $2p_{1/2}$ level[28].The $2p_{3/2}$ level has four degenerated states and its binding energy peak is higher than that of level $2p_{1/2}$, which contains only two spin–orbit (j–j) couplings[28a, 29].

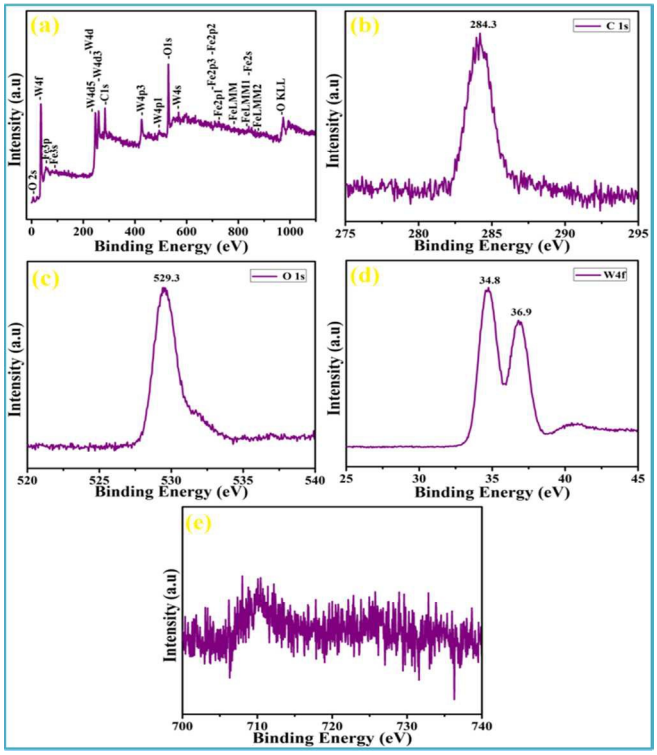

Fig. 5 XPS surface spectra of as-synthesized product: (a) a full-range XPS survey spectrum, (b) C1s peak, (c) O1s peak, (d) W4f doublet peaks, and (e) Fe2p spectrum respectively.

FTIR analysis and BET surface area

Fourier transform infrared (FTIR) spectroscopy was used to further confirm the composition information and chemical bonding present in the as-prepared composite sample as indicated in Fig. 6. Fig. 6represents the typical FTIR spectra of all the samples .Several peaks (749, 820& 965 cm^{-1})existing below 1000 $cm^{-1}$and the broad band observed between 3200-3500 cm^{-1}can be associated with O–W–O stretching modes and O–H stretching vibrations of WO_3[30] respectively. There are several peaks around 1300-1600 cm^{-1}that could be ascribed to H–O–H bending and O–H stretching vibrations of the adsorbed molecules of water on the material surface [31].The peaks below 700 cm^{-1} (*i.e.,*462, 530, 638 and 670 cm^{-1} etc.) can associated with metal-oxygen (Fe–O) stretching vibrational mode of α-Fe_2O_3[32].

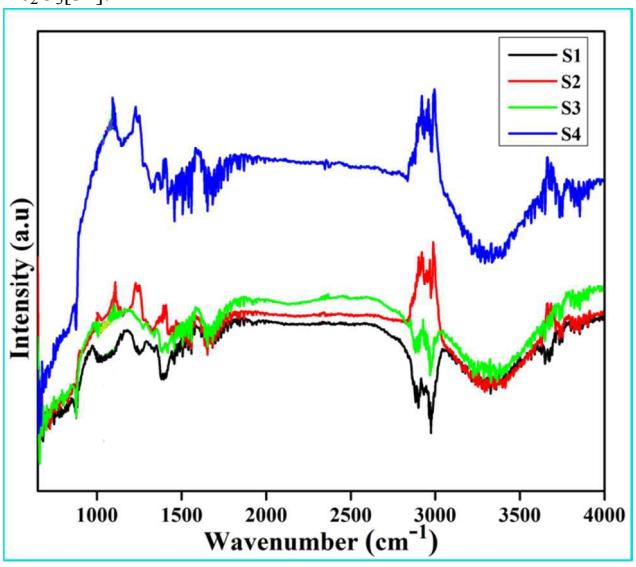

Fig. 6 FTIR spectra of S1-S4 in full range

It has been investigated in many reports [25a, 33] that the large surface area is an important factor for a material to be a good photocatalyst. The high surface area is able to adsorb more organic dyes and provides the increased contact area between dye and catalyst which results in more reactive sites during the photocatalytic reaction. In order to investigate the specific surface area and porous nature of the as-prepared material, N_2 adsorption/desorption isotherm was measured as shown in Fig. 7 (a). The well-known Brunauer–Emmett–Teller (BET) equation [34] was used to calculate specific surface area of the final product in the pressure range 0 to 1 and the specific surface are for porous microplates was estimated as 96.906 m^2/g that possibly would be beneficial for the degradation of organic pollutants. According to IUPAC classification[35], the as-synthesized $WO_3/Fe_2(WO_4)_3$!10.7H_2Oporous microplates exhibit a type IV (P/P_0> 0.3) isotherm with a H2 type hysteresis loop which suggests that the particle size of sample would be in mesoporous range. The pore-size distribution isotherm was obtained by employing Barret–Joyner–Halenda (BJH) method as given in Fig. 7 (b). The peak of pore-size distribution curve (Fig. 7 b) is the centered at 4.664 nm which shows that the fabricated product contains mesoporous structure that would be helpful for adsorption and transition of the dye/or its intermediates during photocatalysis.

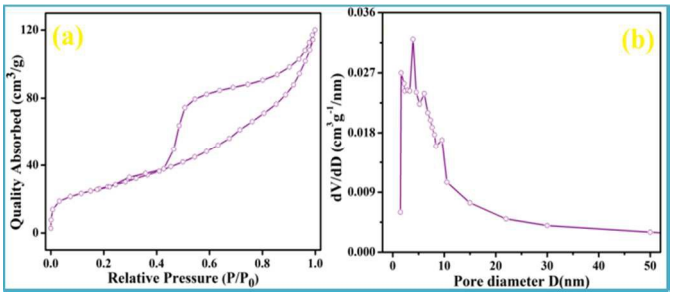

Fig. 7 (a) Nitrogen adsorption-desorption isotherms and (b) pore size distribution of the as-prepared $WO_3/Fe_2(WO_4)_3$!10.7H_2O photocatalyst.

Optical absorption and PL spectra

It is a well-known fact that the range of optical absorption plays an effective role in photocatalysis process, especially for visible-light-driven photodegradation of organic pollutants.The optical absorption spectra of the prepared samples were recorded by UV-VIS-NIR spectrophotometer in the wavelength range 300–800 nm. Fig. 8(a) shows the UV-Vis absorption spectra of all the samples. It can be found that the main absorption edge located at *ca.* 450 nm, so it can be expected that the as-prepared photocatalyst would obviously exhibit enhanced light absorption capability in the visible light region.Using the UV absorption data, the optical band gap $E_g$of all the samples was determined by the following equation

$$(\alpha hv)^{1/2} = A(hv - E_g) \qquad (1)$$

where α denotes the absorption coefficient, $hv$is the photon energy, A is a constant, $E_g$is the band gap energy.

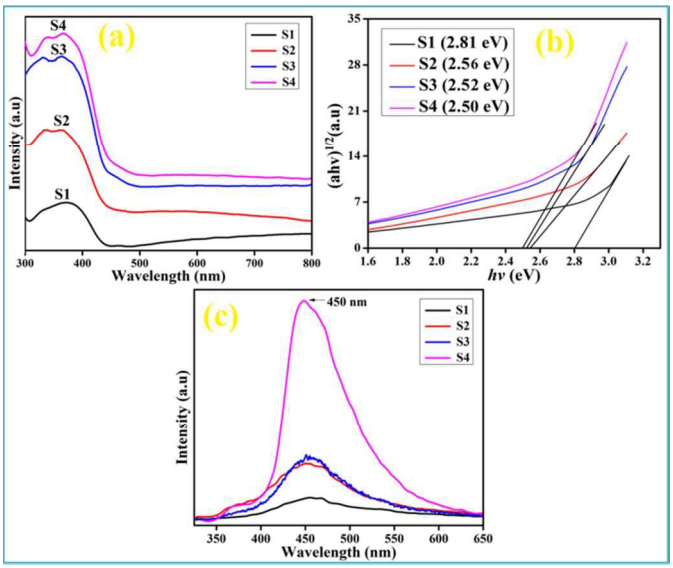

Fig. 8 (a)UV-absorption spectra, (b)corresponding bandgaps, and (c) PL emission spectra of all samples

The band gap energy (E_g) of the synthesized material was calculated from the intercept of the tangent drawn to the curve obtained from the plot of $(\alpha hv)^{1/2}$ versus photon energy (hv). The estimated band gap energies of the samples were calculated as 2.81 and 2.56, 2.52 and 2.50 eVfor the products at 6, 12, 18 and 24 h respectively and

given in Fig. 8 (b). The obtained band gap (2.50 eV) of the final product is thought much favourable for the decontamination of organic dyes under the visible light. Fig. 8 (c) represents the room temperature PL spectra of S1, S2, S3 and S4 and it exhibited a strong blue emission peak positioned at 450 nm which lies in the best optical range and would be favorable for photocatalysis.

Evaluation of photocatalytic properties

The photocatalytic efficiency test of the as-prepared product was evaluated by the photodegradation of MO molecule in the presence of visible light irradiation ($\lambda > 400$ nm).Fig. 9 (a) indicates the graph between $\ln(C_0/C)$ and irradiation time t, where C_0 is the initial absorption of MB when adsorption–desorption equilibrium was established, C represents the absorption at any time t and k is the first-order rate constant. The straight lines indicate that the degradation of MO takes place as a function of irradiation time by fully obeying the first order kinetic fitting. The as-synthesized one-step hybrid $WO_3/Fe_2(WO_4)_3!10.7H_2O$ photocatalyst successfully degraded 96 % of MO in 40 min and exhibited the highest photocatalytic efficiency along with a high reaction rate constant (k=0.06771 min^{-1}) than that of all other products (*i.e.,* at 6, 12 and 18 h) as can be seen in Fig. 9 (a).The samples S1, S2 and S3 took 100, 70 and 60 min for the degradation of MO respectively as can be seen from C/C_0 versus t degradation curves in Fig. 9 (b). In addition, the photocatalytic activities of pure WO_3 and P25 TiO_2 were also evaluated for comparison purpose, which respectively take 140 and 170 minutes to degrade MO. The R^2, known as determination coefficient, has been calculated for each line according to the literature [36]as shown in Fig.9 (c). It provides information about the variability of response, and the value of adjusted R^2 close to 1 means that the predicted values agree with the experimental data. It can be noticed that the value of $R^2$for all samples is greater than 0.95, which implies that the experimental data is in good agreement with the pseudo-first-order model. In Fig. 9 (c), the error bars are displayed corresponding to each value of rate constant. The error bars represents the standard deviations of triplicate experiments. The k values of all other samples (P25 TiO_2, WO_3, S1, S2 & S3) according to pseudo-first-order kinetic equation were respectively calculated as 0.0101, 0.0205, 0.0255, 0.0405 and 0.042 min^{-1} and are given in Fig. 9 (c). From the comparison, it can be noticed that the enhanced photocatalytic performance of the heterostructured system (S4) was 3.3 times greater than pure WO_3 and about 6.7 times greater than that of P25 TiO_2. In addition, the enhanced activity of the photocatalyst was compared to N-doped TiO_2 [37] which was 26 times greater than that of N-doped TiO_2.Fig. 9 (d) represents the photostability/reusability of the as-prepared hybrid sample (S4) for the decomposition of MO. In order to test the stability of the photocatalyst, the recycling photodegradation experiments were performed. For this purpose, the catalyst material used in the first cycle was several times centrifuged with absolute ethanol and DIW , dried at 80 °C and then used it for the next photodegradation cycle. The same steps were carried out for 3rd and 4th cycles. It can be found that the sample S4 presented efficient performance by degrading the dye in the same interval of time even after four times recycling process. Also it can be noted that after recycling four times, only 3 % decline in efficiency was observed that is not a significant loss.

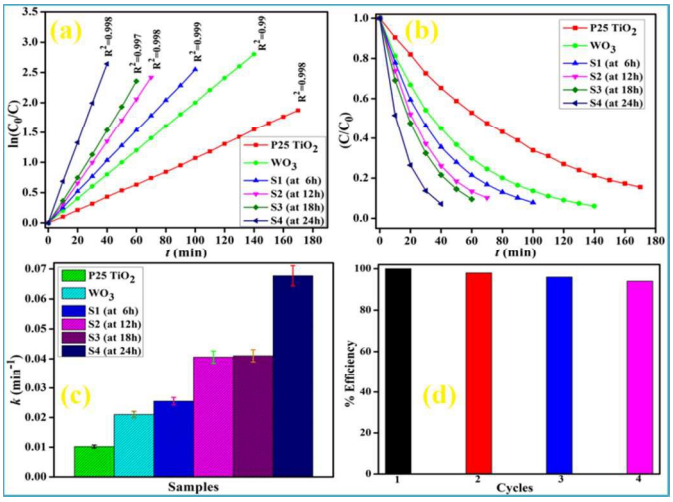

Fig. 9 (a) Plot of ln C_0/C versus irradiation time, (b) C/C_0 versus t degradation curves,(c) k values of all samples, and (d) stability plot of S4.

The explanation for enhanced photocatalytic activity

It is well known fact that the materials with specific morphological structure always exhibit best properties as compared to that of bulk. The photocatalytic process of semiconductor materials generally depends on the photogenerated electrons and holes that migrate to the surface of semiconductors and facilitate as redox sources for degradation of pollutants [1, 38]. For an efficient photocatalytic reaction, the contaminants should possess suitable band potentials for the redox and high ability response to wide light to utilize the maximum irradiated light [38]. However, there are very rare homogeneous semiconductors that have narrow band gaps and suitable redox potentials [40].It has been investigated that hybrid/heterogeneous semiconductors lead to significant absorption shifts in the UV-Vis spectra and also affect the electronic structures of the two materials after coupling. Therefore, it is worth-noting to explore the photocatalytic properties such specially-designed materials in the extended visible spectrum range. The coupling of two different semiconductor oxides with different valence and conduction band potentials provides a vectorial migration of photo-induced electrons and holes from one material to the other. SinceWO_3 and $Fe_2(WO_4)_3!10.7H_2O$ are in close contact to each otherin the as-synthesized one-step $WO_3/Fe_2(WO_4)_3!10.7H_2O$hybrid system, so after exposure to visible light source, the photo-induced electronsstarted to migrate from the conduction band (CB) of$Fe_2(WO_4)_3!10.7H_2O$ to the CB ofWO_3.Simultaneously, a similar migration of photo-induced holes from the valence band (VB) of WO_3 to the VB of $Fe_2(WO_4)_3!10.7H_2O$ was occurred as can be seen in Fig. S3(ESI†). This migration created an excess of positive and negative charges in both the materials due to which a depletion layer was formed at $WO_3/Fe_2(WO_4)_3!10.7H_2O$ interface. This depletion layer inhibited the fast recombination of charge carriers and effectively increased the charge separation efficiency[10, 41]that resulted in the improved photocatalytic activity.

The photocatalytic properties of semiconductors have a very close link with their band-gap energies, chemical composition, crystalline and morphological structure etc. To confirm this fact, the photocatalytic efficiency of the products S1, S2, S3 and S4 (synthesized at different temperatures) were measured under the same conditions. Sample S1 exhibits the lowest degradation performance while the sample S4 (with specific morphology) shows the best efficiency (k=0.06771 min^{-1})as shown in Fig. 9 (c). The comparison shows that the photocatalytic activity increases as the morphological structure of the samples improves. Secondly, the higher specific surface area of the photocatalysts is thought much favorable for photocatalytic process because it provides more possible reactive sites. This is another reason for S4 (96.906 m^2/g) to exhibit enhanced photocatalytic performance.

Besides the above described reasons, it is also worth-noting to evaluate the amount of active species taking part in the photocatalytic reaction. It is well known that during the photo-oxidation reaction, the photo-induced holes in the VB react with surface adsorbed water to produce the hydroxyl radicals (˙OH) [42]. Thus, the photogenerated holes or the formed ˙OH radicals are considered as two main species to oxidize the organic dyes in the aqueous solution[42]. The ˙OH radicals thereby reacting with TA form 2-hydroxyl terephthalic acid (TAOH), that exhibit a characteristic fluorescence peak around 426 nm used as an indirect evidence to monitor the amount of ˙OH radicals [43]. In order to detect the amount of formed ˙OH radicals during the decomposition of MO, we used photoluminescence (PL) technique.

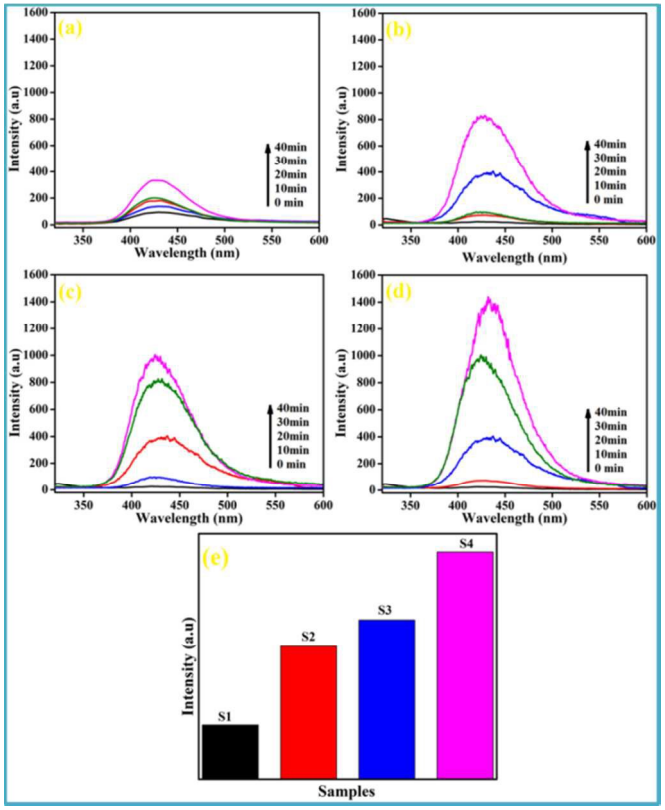

Fig. 10 Fluorescence spectra of 2-hydroxyl terephthalic acid (TAOH) solution generated by (a) S1, (b) S2, (c) S3, (d) S4 for 40 min, and (e) Comparison of the amount of final TAOH generated after 40 min from (a) to (d).

Fig. 10 indicates the fluorescence spectra of TAOH solution in the presence of $WO_3/Fe_2(WO_4)_3!10.7H_2O$with characteristic peak around 426 nm. It be seen that fluorescence peak gradually increase with the increase of irradiation time which is the evidence of formation of hydroxyl radicals .Fig. 10 (a) shows that there are a few ˙OH radicals formed in 60 min for the case of sample S1 and hence it takes longer time to decompose the dye which in good agreement with the photocatalytic activity of S1 (Fig. 9 a). From Fig. 10 (b & c), it can be noted that the formed ˙OH radicals increased for samples S2 & S3 and there are maximum ˙OH radicals formed when the final product (S4) is used along with TAOH solution (Fig. 10 d) suggesting the excellent capability of $WO_3/Fe_2(WO_4)_3!10.7H_2O$ for the decomposition of MO. Fig. 10 (e) indicates the comparison of the amount of TAOH generated after an irradiation time of 40 min.

In summary, the remarkable visible-light photocatalytic activity of the as-synthesized one-step $WO_3/Fe_2(WO_4)_3!10.7H_2O$ hybrid can be attributed to the following factors: (i) the as-synthesized microplates contains porous structure that is helpful to adsorb more reactive species, (ii) the two semiconductors combined with each other by a single step hydrothermal treatment led to significant absorption shifts in the UV-Vis spectra spectra which was much favourable for photocatalysis, (iii) the larger specific surface area (96.906 m^2/g) provided more reactive sites to adsorb more organic pollutants, (iv) the effective formation of ˙OH radicals, and finally (v) the synergistic effect between two materials due to coupling provided the efficient photo-induced electron–hole pairs separation.

Conclusions

We have demonstrated a highly efficient visible-light-driven$WO_3/Fe_2(WO_4)_3!10.7H_2O$ photocatalyst by simple one-step hydrothermal technique. This unique hybrid photocatalyst presented significantly improved light harvesting, photogenerated charge separation and transfer of charge carriers due to the synergistic effect at the heterojunction interface. The fabricated material with special structural features, high specific surface area and effective generation of ˙OH radicals leads to remarkable photocatalytic activity towards the decomposition of MO under visible light irradiation.The enhanced photocatalytic acitivity of the sample was compared with pure WO_3 and P25 TiO_2, which was about 3.3 and 6.7 times greater than that of pure WO_3 and P25 TiO_2.It is believed that the synthesized photocatalyst would be advantageous for high activity and low cost with its promising practical applications in water purification.

Acknowledgements

This work was supported by National Natural Science Foundation of China (23171023，50972017) and the Research Fund for the Doctoral Program of Higher Education of China (20101101110026).

Notes and references

[a]Research Centre of Materials Science, Beijing Institute of Technology, Beijing 100081, P. R. China.

[b]Department of Physics, Government College University Faisalabad, 38000, Faisalabad Pakistan.

† Footnotes should appear here. These might include comments relevant to but not central to the matter under discussion, limited experimental and spectral data, and crystallographic data.

Electronic Supplementary Information (ESI) available: [Synthesis of pure WO_3, TG analysis of the composite sample, synthesis of $Fe_2(WO_4)$ it UV-absorption, bandgap calculation and proposed mechanism for photogenerated charge carriers in $WO_3/Fe_2(WO_4)_3!10.7H_2O$]. See DOI: 10.1039/b000000x/

1. M. R. Hoffmann, S. T. Martin, W. Choi and D.W. Bahnemann, *Chem. Rev.,* 1995, **95**, 69.
2. S. C. Zhang, J. D. Shen, H. B. Fu, W. Y. Dong, Z. J. Zheng and L. Y. Shi, *J. Solid State Chem.,* 2007, **180**, 1456.
3. A. Fujishima and K. Honda, *Nature*, 1972, **238**, 37.
4. H. Choi, A. C. Sofranko and D. D. Dionysiou, *Adv. Funct. Mater.,* 2006, **16**, 1067.
5. S. Sakthivel, S. U. Geissen, D. W. Bahnemann, V. Murugesan and A. Vogelpoph, *J. Photochem. Photobiol., A,* 2002, **148**, 283.
6. A. Ponzoni, E. Comini, G. Sberveglieri, J. Zhou, S. Z. Deng, N. S. Xu, Y. Ding and Z. L. Wang, *Appl. Phys. Lett.,* 2006, **88**, 203101.
7. S. Baeck, K. Choi, T. F. Jaramillo, G. D. Stucky and E. W. McFarland, *Adv. Mater.,* 2003, **15**, 1269.
8. C. Santato, M. Odziemkowshi, M. Ulmann and J. Augustynski, *J. Am. Chem. Soc.,* 2001, **123**, 10639.
9. J. Zhou, L. Gong, S. Z. Deng, J. Chen, J. C. She, N. S. Xu, R. Yang and Z. L. Wang, *Appl. Phys. Lett.,* 2005, **87**, 223108.
10. Z. G. Zhao and M. Miyauchi, *Angew. Chem. Int. Ed.,* 2008, **47**, 7051.
11. (a) H. T. Zheng and M. Mathe, *Int. J. Hydrogen Energy,* 2011, **36,** 1960; (b) V. Chakrapani, J. Thangala and M. K. Sunkara, *Int. J. HydrogenEnergy*, 2009, **34**, 9050.
12. (a) D. Chen and J. H. Ye, *Chem. Mater.,* 2007, **19**, 4585; (b) C. Z. Wu, L. Y. Lei, X. Zhu, J. L. Yang and Y. Xie, *Small,* 2007, **3**, 1518; (c) J. Q. Yu and A. Kudo, *Adv. Funct. Mater.,* 2006, **16**, 2163.
13. T. Arai, M. Horiguchi, M. Yanagida, T. Gunji, H. Sugihara and K. Sayama, *Chem. Commun.,* 2008, 5565.
14. K. Hong, K. Kim, S. Kim, I. Lee, H. Cho, S. Yoo, H. W. Choi,N. Y. Lee, Y.-H. Tak and J. L. Lee, *J. Phys. Chem. C,* 2011, **115**, 3453.
15. M. Miyauchi, *Phys. Chem. Chem. Phys.,* 2008, **10**, 6258.
16. T. Huang, X. Lin, J. Xing, W. Wang, Z. Shan and F. Huang, *Mater. Sci. Eng., B,* 2007, **141**, 49.
17. J. P. Chen and R. T. Yang, *Appl. Catal., A,* 1992, **80**, 135.
18. Z. Liu, Z. G. Zhao and M. Miyauchi, *J. Phys. Chem. C,* 2009,**113**, 17132.
19. (a) Imran Aslam, Chuanbao Cao, M. Tanveer, Waheed S. Khan, Muhammad Tahir, M. Abid, Faryal Idrees, Faheem K. Butt, Zulfiqar Ali and Nasir Mahmood, *New J. Chem.,* 2014, **38**, 5462; (b) F. Idrees, C. Cao, F. K. Butt, M. Tahir, M. Tanveer, I. Aslam, Z. Ali, T. Mahmood and J. Hou, *CrystEngComm,* 2013, **15**, 8146; (c) M. Tanveer, C. Cao, W. S. Khan, Z. Ali, I. Aslam, F. K. Butt, F. Idrees, M. Tahir and N. Mahmood, *CrystEngComm,* 2014, **16**, 5290; (d) M. Tanveer, Chuanbao Cao,Imran Aslam, Zulfiqar Ali, Faryal Idrees, Muhammad Tahir, Waheed S. Khan, Faheem K. Butt and Asif Mahmood, *RSC Adv.,* 2014, **4**, 63447.
20. (a) Imran Aslam, Chuanbao Cao, M. Tanveer, M. Hassan Farooq, Waheed S. Khan, Muhammad Tahir, Faryal Idrees and Syed Khalid, *RSC Adv.,* 2015, **5**, 6019; (b) (b) M. Tahir, C. Cao, F. K. Butt, S. Butt, F. Idrees,Z. Ali, I. Aslam, M. Tanveer, A. Mahmood and N. Mahmood, *CrystEngComm,* 2014, **16**, 1825; (c) M. Tahir, C. Cao, F. K. Butt, F. Idrees, N. Mahmood, Z. Ali, I. Aslam, M. Tanveer, M. Rizwan and T. Mahmood, *J. Mater. Chem. A,* 2013, **1**, 13949; (d) Muhammad Tanveer, Chuanbao Cao, Imran Aslam, Zulfiqar Ali, Faryal Idrees,Waheed Samraiz Khan, Muhammad Tahir, Syed Khalid, Ghulam Nabi andAsif Mahmood, *NewJ.Chem.,* 2015, **39**, 1459.
21. Suk Joon Hong, Seungok Lee, Jum Suk Jang and Jae Sung Lee, *Energy Environ. Sci.,* 2011, **4**, 1781.
22. Shouli Bai, Kewei Zhang, Jianhua Sun, Ruixian Luo, Dianqing Li and Aifan Chen, *CrystEngComm,* 2014, **16**, 3289.
23. (a) H. Zhang, X. J. Lv, Y. M. Li, Y. Wang and J. H. Li, *ACS Nano* 2010, **4**,380; (b) O. K. Varghese, M. Paulose, T. J. LaTempa and C. A. Grimes, *Nano Lett.,* 2009, **9**, 731; (c) K. Woan, G. Pyrgiotakis and W. Sigmund, *Adv. Mater.,* 2009, **21**, 2233; (d) J. Zhang, Q. Xu, Z. C. Feng, M. J. Li, C. Li, *Angew. Chem.*, 2008,**120**, 1790; (e) H. Tada, T. Kiyonaga and S. Naya, *Chem. Soc. Rev.,* 2009, **38**, 1849.
24. (a) G. Zhang, X. Shen and Y. Yang, *J. Phys. Chem. C,* 2011, **115**,7145; (b) J. Liu, T. Luo, S. T. Mouli, F. Meng, B. Sun, M. Li andJ. Liu, *Chem. Commun.,* 2010, **46**, 472; (c) J. Liu, H. Xia, L. Luand D. Xue, *J. Mater. Chem.,* 2010, **20,** 1506; (d) N. Sutradhar,A. Sinhamahapatra, S. K. Pahari, M. Jayachandran,B. Subramanian, H. C. Bajaj and A. B. Panda, *J. Phys.Chem. C,* 2011, **115**, 7628; (e) N. Sutradhar,A. Sinhamahapatra, S. K. Pahari, P. Pal, H. C. Bajaj,I. Mukhopadhyay and A. B. Panda, *J. Phys. Chem. C,* 2011,**115**, 12308.
25. (a) I. Aslam, C. Cao, W. S. Khan, M. Tanveer, M. Abid, F. Idrees,R. Riasat, M. Tahir, F. K. Butt and Z. Ali, *RSC Adv.,* 2014, **4**,37914; (b) Jiefu Yin, Huaqiang Cao, Jingxian Zhang, Meizhen Qu, and Zhongfu Zhou, *Cryst. Growth Des.,*2013, **13**, 759.
26. (a) G. Liu, P. Niu, C. Sun, S. C. Smith, Z. Chen, G. Q. (Max) Lu and H. Cheng, *J. Am. Chem. Soc.,* 2010, **132**, 11642; (b) R. Marschall, A. Mukherji, A. Tanksale, C. Sun, S. C. Smith, L. Wang and G. Q. (Max) Lu, *J. Mater. Chem.,* 2011, **21**, 8871, (c) Gang Liu, Ping Niu, Chenghua Sun, Sean C. Smith, Zhigang Chen,Gao Qing (Max) Lu, and Hui-Ming Cheng, *J. Am. Chem. Soc.,* 2010, **132**, 11642.
27. (a) M. Sun, N. Xu, Y. W. Cao, J. N. Yao and E. G. Wang, *J. Mater. Res.,* 2000, **15**, 927; (b) B. A. Deangelis and M. Schiavello, *J. Solid State Chem.,* 1977, **21**, 67; (c) A. P. Shpak, A. M. Korduban, M. M. Medvedskij and V. O. Kandyba, *J. Electron Spectrosc. Relat. Phenom.,* 2007, **156**, 172.
28. (a) A. A. Tahir, K. G. U. Wijayantha, S. Saremi-Yarahmadi, M. Mazhar and V. McKee, *Chem. Mater.,* 2009, 21, 3763; (b) S. Yang, C. Wang, L. Ma, Y. Peng, Z. Qu, N. Yan, J. Chen, H. Chang and J. Li, *Catal. Sci. Technol.,* 2013, **3**, 161.
29. T. Yamashita and P. Hayes, *Appl. Surf. Sci.,* 2008, **254**,2441.
30. (a) C. Guery, F. Choquet, J. Dujeancourt, M. Tarascon andJ. C. Lassegues, *J. Solid State Electrochem.,* 1997, **1**, 199; (b) C. Jan´aky, N. R. de Tacconi, W. Chanmanee and K. Rajeshwar, *J. Phys. Chem. C,* 2012, **116**, 19145; (c) A. Baserga, V. Russo, F. Difonzo, A. Bailini, D. Cattaneo,C. Casari, A. Libassi and C. Bottani, *Thin Solid Films,* 2007, **515**, 6465; (d) Z. J. Gu, T. Y. Zhai, B. F. Gao, X. H. Sheng, Y. B. Wang, H. B. Fu, Y. Ma and J. N. Yao, *J. Phys. Chem. B,* 2006, **110**, 23829; (e) W. Jiang, M. Pelaez, D. D. Dionysios, M. H. Entezari, D. Tsoutsou and K. O'Shea, *Chem. Eng. J.,* 2013, **222**, 533.
31. (a) S. Kumar, T. Surendar, A. Baruah and V. Shanker, *J. Mater.Chem. A,* 2013, **1**, 5333; (b) H. I. S. Nogueira, A. M. V. Cavaleiro, J. Rocha, T. Trindade and J. D. P. D. Jesus, *Mater. Res. Bull.,* 2004, **39**, 683; (c)Y. D. Wang, C. L. Ma, X. D. Sun and H. D. Li, *Nanotechnology,*2002, **13**, 565.

32. (a) G. K. Pradhan and K. M. Parida, *ACS Appl. Mater. Interfaces,* 2011,**3,** 317; (b) R. Sharma, S. Lamba and S. Anna Poorni, *J. Phys. D: Appl. Phys.,* 2005, **38**, 3354.
33. (a) C. Ye, Y. Bando, G. Shen and D. Golberg, *J. Phys. Chem. B,* 2006, **110**, 15146. (b) R. Narayanan and M. A. El-Sayed, *Nano Lett.,* 2004, **4,**1343.
34. S. Brunauer, P. H. Emmett and E. Teller, *J. Am. Chem. Soc.,*1938, **60**, 309.
35. K. S. W. Sing, *Pure Appl. Chem.,* 1985, **57**, 603.
36. W. Jiang, J. A. Joens, D. D. Dionysiou and K. E. O'Shea, *J. Photochem. Photobiol., A,* 2013, **262**, 13.
37. Xiaoyan Zhang and Xiaoli Cui, *RSC Adv.,* 2014, **4**, 60907.
38. (a) A. Mills and S.L. Hunte, *J.Photochem. Photobiol. A: Chem.*1997, **108,** 1;(b) D.S. Bhatkhande, V.G. Pangarkar and A. ACM Beenackers, *J. Chem. Technol. Biotechnol.,*2002, **77,** 102.
39. (a) A. Kudo and Y. Miseki, *Chem. Soc. Rev.,*2009, **38,** 253;(b) K. Maeda, *J. Photochem. Photobiol. C: Photochem. Rev.*,2011, **12,** 237.
40. (a) M.W. Kanan, D.G. Nocera, *Science,*2008, **31,** 1072; (b) O. Khaselev and J.A. Turner, *Science,*1998, **280**, 425; (c) Z. G. Zou, J. H. Ye, K. Sayama and H. Arakawa, *Nature,*2001, **414**, 625; (d) J. S. Jang, H. G. Kim and J.S. Lee, *Catal. Today,*2012, **185,** 270.
41. Sun S M, Wang W Z, Zeng S Z, Shang M and Zhang L,*J. Hazards. Mater.,* 2010,**178,**427.
42. A. L. Linsebigler, G. Lu and J. T. Yates, *Chem. Rev.,* 1995, **95**, 735.
43. T. Hirakawa and Y. Nosaka, *Langmuir,* 2002, **18**, 3247.

TOC

First time synthesized novel microplates of $WO_3/Fe_2(WO_4)_3!10.7H_2O$ by a one-step hydrothermal technique. The as-prepared photocatalyst maintained a high specific surface area (96.906 m^2/g) and showed excellent photocatalytic activity (k=0.06771 min^{-1}) for the degradation of methyl orange.